Hindawi
Journal of Chemistry
Volume 2023, Article ID 7011995, 14 pages
https://doi.org/10.1155/2023/7011995

Research Article

Evaluation of Pb (II) Removal by Tea Pulp Modified with Magnetite Nanoparticle

Morteza Mozaffari,[1] Abbas Khodabakhshi ,[2] and Amin Azizi[3]

[1]*Department of Physics, Faculty of Science, University of Isfahan, Isfahan, Iran*
[2]*Department of Environmental Health Engineering, School of Health, Shahrekord University of Medical Sciences, Shahrekord, Iran*
[3]*Organization of Engineers of Chaharmahal and Bakhtiari Province, Shahrekord, Iran*

Correspondence should be addressed to Abbas Khodabakhshi; khodabakhshi16@gmail.com

Received 29 November 2022; Revised 21 January 2023; Accepted 1 February 2023; Published 23 February 2023

Academic Editor: Samuel Lalthazuala Rokhum

Tea waste was used to successfully synthesize magnetic nanoparticles (TWMNPs). In this investigation, Pb (II) was eliminated by tea waste modified with magnetite nanoparticles (TWMNPs) was investigated. To prepare the TWMNPs, $FeCl_3.6H_2O$ was dissolved in double distilled water (DDW) and 20 g of pulp tea was added slowly and stirred, after 30 min TWMNPs adsorbent were separated through an external magnetic field and washed three times with double distilled water (DDW) and ethanol then dried at 60°C. The FESEM test of TWMNPs shows the particle size in the range of 15–20 nm and spherical/cuboid-shaped crystal structure of Fe_3O_4 (magnetite). X-ray analysis showed that the main XRD diffraction peaks of TWMNPs are related to Fe_3O_4, HighScore plus X'Pert software was used to identify the phase in this sample. The specific surface area of the prepared magnetite nanoparticles was 25.2 $m^2.g^{-1}$. The pore volume, maximum pore radius, and VSM of TWMNPs were 14.4 $cm^3.g^{-1}$, 2.3 nm, and 3.37–2.41, respectively. The effects of various parameters, such as contact time, pH, concentration, and adsorbent dosage, were studied. The experimental isotherm data were analyzed using the Langmuir and Freundlich models, and it was found that the removal process followed the Langmuir isotherm and the maximum adsorption capacity calculated by Langmuir fitting was 10.67 $mg.g^{-1}$. In addition, the adsorption kinetics followed the first-order kinetic model and the value of rate constant was found to be 14.04×10^{-2} min^{-1}. The results showed that increasing the pH level led to a rise in the response level and Pb (II) removal. Also, the trend in Pb (II) removal and response level had an increase with increasing the initial concentration of Pb (II). Increasing contact time from 5 to 20 minutes has a slight effect on Pb (II) removal. Considering the results, TWMNPs could lead to suitable results for the removal of Pb (II) from wastewater containing this metal. And the maximum adsorption capacity was found to be 10.67 $mg.g^{-1}$.

1. Introduction

Today, the increase and development of industrial activities have led to an increment in the production of industrial wastewater containing toxic heavy metals such as Pb (II), Hg, and As [1]. These elements are nonbiodegradable and tend to accumulate in the human body and living organisms, which can cause many diseases and disorders [2–4].

Heavy metal contaminations could exist in wastes of many industries, such as metal plating, mining operations, tanneries, chloralkali, radiator manufacturing, smelting, and alloy industries as well as storage battery industries [5]. Lead is a heavy, soft, malleable, bluish grey metal [6]. Lead is of particular interest, because of its toxicity and its widespread presence in the environment [7]. Lead is a well-known highly toxic metal considered as a priority pollutant [8]. It is an industrial pollutant, which enters the ecosystem through soil, air, and water.

Among heavy metals, Pb (II) is widely used in industries and is the fifth most consumed metal in the world [9]. The main industries producing Pb (II) in the environment are incineration, metallurgy, mineral exploration, and lead-acid

batteries [10, 11]. Lead has destructive and irreversible effects on the ecosystem [12, 13]. Lead dissolves at acidic pH and precipitates at alkaline conditions and can enter the body through water and food ingested and through respiration. Once ingested, Pb (II) will be changed to biotoxic compounds by biomolecules in the proteins and enzymes. As a result, their structure changes, and their biological interactions become difficult [14]. The presence of high levels of lead in the environment may cause long-term health risks to humans and ecosystems [6, 15] The World Health Organization (WHO) has established 0.05 $mg.L^{-1}$ as the maximum permissible limit (MPL) for lead in drinking water. The Environmental Protection Agency (EPA) has established a permissible limit ($mg.L^{-1}$) for Pb (II) in wastewater of 0.05 $mg.L^{-1}$ [5]. In industrial wastewaters, lead-ion concentrations approach 200–500 $mg.L^{-1}$, which are very high values in comparison to those are acceptable to reach water quality standards. So, the lead-ion concentration of wastewaters must be reduced by proper treatments to an acceptable level of 0.05–0.10 $mg.L^{-1}$, before discharging to waterways or sewage systems [5]. So far, various methods, such as precipitation, ion exchange, surface adsorption, reverse osmosis, electrocoagulation, cementation, electrodialysis, electrowinning, and membrane processes, have been used to remove Pb (II) from an aqueous media [16, 17].

These methods for removing heavy metals are associated with high initial costs, high operating and maintenance costs, the need for the ability and skill of the operator, and high energy consumption [16, 17]. Also, if the reaction between the chemicals and the metal is not complete, there is a possibility of increased secondary contamination. Another disadvantage of these methods is the production of sludge, the disposal of which will impose significant costs on the system [17].

An effective and useful method to reduce these disadvantages is the magnetization of adsorbents using metal oxides or magnetic nanoparticles [18]. In this method, the adsorbent along with the adsorbed contaminants can be separated from the aqueous medium by an external magnetic field easily and quickly. On the other hand, magnetic nanosorbents have better performance than conventional magnetic microsorbents due to their high specific surface area and low internal dispersion resistance [19]. Due to their surface area and more active sites, nanoparticles show appropriate adsorption efficiency for interaction with metal species and can be easily synthesized [20].

Magnetite is a magnetite iron oxide with the chemical formula of Fe_3O_4. This compound has significant properties compared to other iron oxides and hydroxides, due to the presence of iron cations in two capacities (Fe^{2+} and Fe^{3+}), and it is very strong compared to other adsorbent iron oxides and has an extraordinary magnetic property [21]. These compounds fall into the category of nanoparticles when their size is less than 100 nm. Usually, iron oxide nanoparticles' specific surface area is more than 100 $cm^2.g^{-1}$, these two properties, (1) the surface-area-to-volume ratio and (2) high adsorption capacity, have attracted the attention of researchers to these particles [22].

In recent years, the use of some plants or their extracts such as tea, green tea, coffee, and corn bran due to their unique properties and lack of harmful and hazardous compounds for the environment has been proposed to improve the surface and synthesis of iron nanoparticles [23]. The use of new technologies such as nanoparticles in the removal of Pb (II) is very important due to the lack of defects in conventional methods and its low cost [24]. A study by Wang et al. showed the removal of 90% of Pb (II) from the aqueous medium using graphene oxide chitosan adsorbent. The study of Lunge et al. showed that iron oxide prepared from tea waste has a good ability to remove arsenic ions from water and is cost-effective [25].

The main objective of the present study was to evaluate the effects of adding tea waste treated magnetite nanoparticles (TWMNPs) to find a solution for the removal of lead (II) from aqueous solutions.

2. Materials and Methods

2.1. Chemicals and Reagents. All chemicals and reagents used were of analytical grade and supplied by Merck. The chemicals used in this study were lead nitrate, ferric chlorides, ammonia solution, acetone, hydrochloric acid, ethanol, and sodium hydroxide. A stock solution of lead (II) was prepared by dissolving lead nitrate (purchased from Merck) in double distilled water. Working solutions were obtained by diluting the stock solution with double distilled water (DDW). Fresh dilutions were prepared and used for each experiment. Hydrochloric acid and sodium hydroxide (purchased from Merck) were used to adjust the pH.

2.2. Preparation Adsorbent. The chemical coprecipitation technique has been used to prepare particles with homogeneous composition and narrow size distribution [20, 26, 27]. This technique is probably the most common and efficient method to obtain magnetic particles. A complete precipitation of Fe_3O_4 was achieved under alkaline condition, while maintaining a molar ratio of Fe^{2+} to Fe^{3+}, 1 : 2, under an inert environment. To obtain 4 g of magnetic particles, 4.2 g of $FeSO_4{\cdot}7H_2O$ and 6.2 g of $FeCl_3{\cdot}6H_2O$ were dissolved under the inert atmosphere in 160 mL of double distilled water with severe stirring. While the solution was heated to 80°C, 20 mL of ammonium hydroxide solution (25%) was added. To ensure complete growth of the nanoparticle crystals, the solution was then added to 20 g of tea waste, and the reaction was carried out for 30 min at 80°C under constant stirring.

The resulting suspension was cooled down to room temperature and then repeatedly washed with double distilled water (DDW) to remove unreacted chemicals. TWMNPs adsorbent were separated through an external magnetic field and washed three times with double distilled water (DDW) and ethanol and dried at 60°C [20, 28]. The reactions that occur in the production of magnetic nanoparticles TWMNPs are as shown in equations (1) and (2), [20, 26, 27].

$$FeSO_4{\cdot}7H_2O + 2FeCl_3{\cdot}6H_2O + 8NH_4OH \longrightarrow Fe_3O_4 + 6NH_4Cl + (NH4)_2\,SO_4 + 17H_2O, \quad (1)$$

$$Fe_3O_4 + TW + 17H_2O \longrightarrow TW{-}Fe_3O_4\,(\text{TWMNPs}). \quad (2)$$

2.3. Adsorbent Analysis Methods. Tea waste magnetite nanoparticles (TWMNPs) were identified by using BET, SEM, VSM, and XRD. N_2 gas was used as the adsorbent, and the specific surface area and porosity analyzer PHS-1020 (PHS-China) was used to measure the BET (Brunauer–Emmett–Teller) surface areas of the adsorbent materials.

Barrett–Joyner–Halenda (BJH) and micropore (MP) methods were based on the measurement of the volume of nitrogen gas surface adsorption and desorption at 77 K. The surface morphology of the magnetite nanoparticles was evaluated using a field emission scanning electron microscope (FESEM-LEO 1450 Vp Germany), and in order to measure magnetic properties of the nanoparticles, a vibrating sample magnetometer (Meghnatis Daghigh Kavir Kashan Co. Kashan, Iran) was used.

The composition of the materials was identified by X-ray diffraction (XRD) (Philips, X-Pert Pro, Netherland), and this instrument was equipped with copper anode generating (Cu-K_α) radiation (λ = 1.5406 Å).

2.4. Adsorption Experiment. The experiments were designed by response surface methodology (RSM) in central composite design (CCD). To design the experiments with the central composite design method, the minimum and maximum levels were entered into the design expert software, and other levels among the minimum and maximum points were determined by the software. Finally, 5 levels were determined for the parameters. The number of tests in design expert software was obtained from the following relationship:

$$N = 2^K + 2k + C_0, \quad (3)$$

where N refers to the number of experiments, k is the number of parameters, and C_0 represents the number of central points. In this study, a total of 30 experiments were obtained with 4 parameters including time, adsorbent concentration, pollutant concentration, and pH, and six tests at the central point.

The variables were initial lead concentration, pH, adsorbent dosage, and contact time. The adsorption of Pb (II) on tea waste magnetite nanoparticles (TWMNPs) was studied by a batch technique. Synthetic industrial wastewater was prepared by dissolving lead nitrate ($Pb(NO_3)_2$) in deionized double distilled water (DDW). The adsorption study was performed using 100 ml of the synthetic wastewater at room temperature. The adsorption study was performed by varying the pH (2, 3.5, 5, 6.5, and 8), initial contaminant concentration (0.1, 0.5, 1, and 2 g L^{-1}), contact time (5, 10, 15, and 20 minutes), and magnetite nanoparticle concentration (0.5, 1, 2, and 5 g.L^{-1}) factors.

After adjusting the pH of the samples, the required adsorbent was added to each sample, and based on the designed time, it was stirred by a shaker at 150 rpm. The magnetite nanoparticles were separated by two strong magnets and filtered. The remaining Pb (II) concentration in the solution was measured by anatomic absorption spectroscopy(AAS), Varian-240 (USA), the limit of detection (LoD) and limit of quantity (LoQ) for this device are equal to 14 and 46.66 μg.L^{-1}, respectively.

2.5. Analysis. Samples were analyzed by a atomic absorption spectroscopy (AAS), Varian-240 (USA), then removal efficiency of Pb (II) was determined. Equation (3) was used for the calculation.

$$R = \frac{C_0 - C_e}{C_0} \times 100, \quad (4)$$

where R refers to the removal efficiency and C_0 and C_e represent the initial and final metal ion concentration (mg/L). The quantity of Pb (II) adsorbed on tea waste magnetite nanoparticles (TWMNPs) was calculated using the following well-known equation. The quantity of Pb (II) adsorbed on tea waste magnetite nanoparticles (TWMNPs) was calculated using the following equation:

$$q_e = \frac{V(C_0 - C_e)}{m}, \quad (5)$$

where q_e (mg/g) and C_e (mg/L) are the amount of Pb (II) adsorbed and the equilibrium concentration, respectively.

3. Results and Discussion

3.1. Characterization of Pulp Tea Modified with Magnetite Nanoparticles

3.1.1. FESEM and XRD Analysis. The FESEM test was used to examine the microstructure of samples synthesized at temperatures of 400 and 450°C, and the results are shown in Figure 1.

According to Figure 1 and the micrographs with higher magnification, it is clear that in both of these samples, particles with a pseudospherical morphology and different sizes can be seen, and these particles are probably the same iron oxide particles complexed with the compounds in tea waste.

By comparing the micrographs visible in Figures 1(c) and 1(d), it is clear that the size of the particles in the sample synthesized at a higher temperature is larger than the particles visible in the micrograph corresponding to the sample synthesized at a lower temperature. In order to measure the particles more accurately and to check the size distribution of visible particles in these micrographs, 100

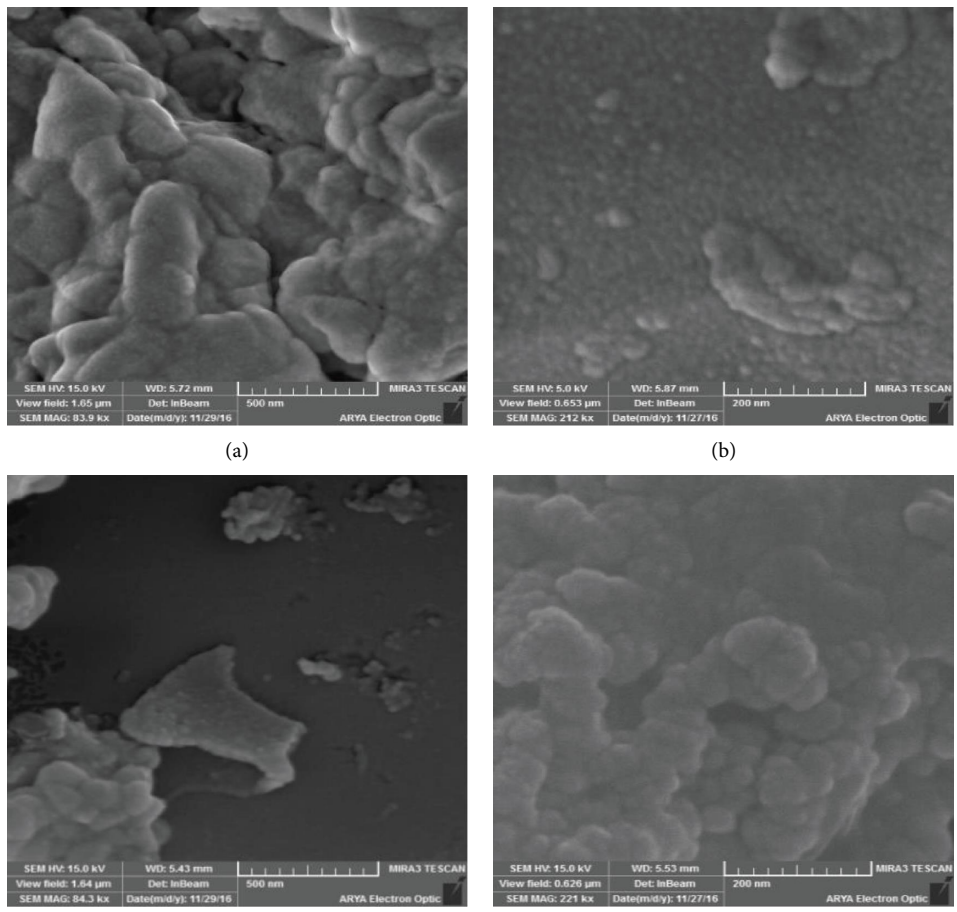

Figure 1: FESEM images tea treated pulp magnetite nanoparticles at temperatures of 400 (a and b) and 450°C (c and d) and different magnifications.

particles from each sample were measured for the size using the *J* image processing software.

The particle size distribution diagrams as well as the statistical parameters extracted from these measurements are shown in Figure 2 and Table 1, respectively.

According to the histogram shown in Figure 2, in the sample synthesized at a temperature of 400°C, among the 100 measured particles, about 50% of the particles have a diameter between 15 and 20 nm, and this size range has the largest number of particles. In the histogram of the sample synthesized at a temperature of 450°C, the size of the particles located in the size range of 20 to 30 nm has the largest number of particles (about 30% of all particles). It is also clear from these histograms that the particle size distribution in the 450°C sample is much wider than the particle size distribution in the 400°C sample. Wide distribution of the particle size means greater difference in particle size than the average value. Therefore, in the sample synthesized at 450°C, the particles have a greater distance with the calculated mean diameter. According to Table 1, with the increase in the synthesis temperature, the mean diameter of the particles increased from 18.6 ± 7.2 nm at 400°C to 36.3 ± 12.8 nm for the sample synthesized at 450°C. This increase in size is due to greater growth. Nanoparticles located at a higher temperature. The X-ray diffraction pattern of the investigated sample is shown in Figure 3.

HighScore plus X'Pert software was used to identify the phase in this sample. According to Figure 3, it is clear that on the XRD pattern of the sample, there is a broad hump on the pattern's background between 20 and 40 degrees, which can be due to the presence of organic compounds in the tea pulp that have a noncrystalline (amorphous) structure. In addition, on the diffraction pattern, there are some sharp peaks related to the magnetite phase (Fe_3O_4), reference code JCPDS no. 96-900-5840, with a cubic crystal structure and a space group of Fd-3m. On the pattern, 28.5, 30.3, 35.7, 43.2, 57.1, and 62.8° diffraction peaks are related to the diffraction planes (002), (220), (311), (400), (511), and (440), respectively [29]. Scherrer's equation is used to find the mean crystallite size [30]:

$$D = \frac{k\lambda}{(\text{FWHM}) \times \cos(\theta)}. \quad (6)$$

In this equation, D is the mean crystallite size, k is the shape factor, λ is the wavelength of the X-ray used (1.5406 Å), FWHM is the bandwidth at half height, and θ is the location of the peak. Having the value of cos (θ) and

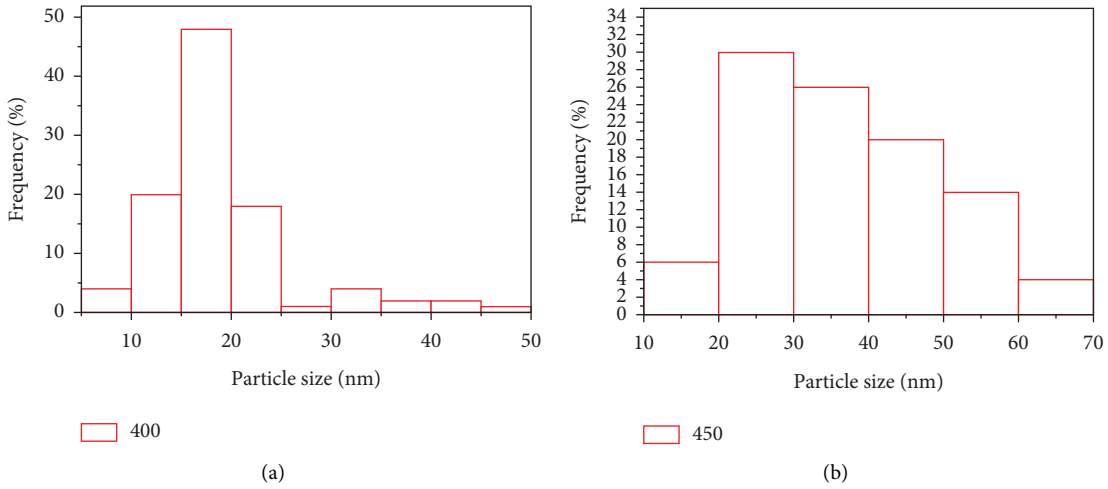

Figure 2: Histograms of particle size distribution in micrographs of tea waste magnetic nanoparticles at (a) 400 and (b) 450°C.

Table 1: Statistical results of histograms of magnetite nanoparticles.

Sample	Total number of measurements	Mean (nm)	Standard deviation (nm)	Smallest particle size (nm)	Largest particle size (nm)
400	100	18.6	7.2	8.4	45.8
450	100	36.3	12.8	34.7	68.1

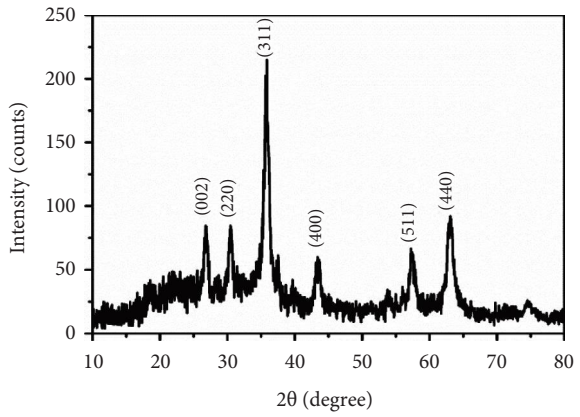

Figure 3: X-ray diffraction pattern of tea treated pulp magnetite nanoparticles.

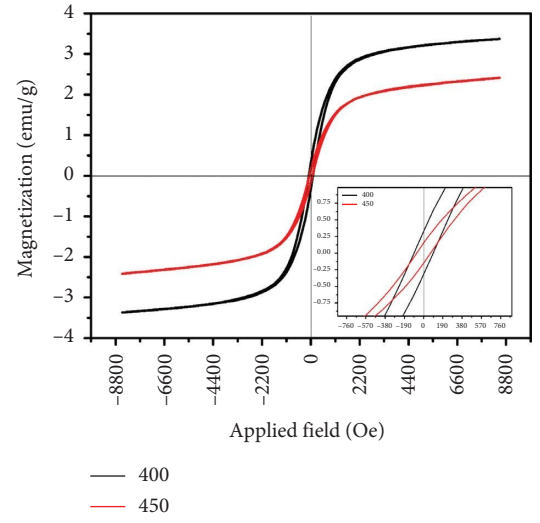

Figure 4: Variations of the magnetization with respect to applied magnetic field of the samples heated at 400 and 450°C. Inset shows the low field part of the curves.

FWHM as well as the fixed values of λ (1.5406 Å) and k (0.9), the value of the crystal size is obtained according to Scherrer's equation, which considering that λ was in angstroms, this value is also in angstroms. The crystal size in nanometers is calculated by dividing the obtained value by 10. This parameter for the magnetite phase is equal to 16.8 nm.

3.2. VSM Analysis. Magnetic properties of the TWMNPs were evaluated by plotting their magnetizations versus applied magnetic field, Figure 4. The maximum applied field (H_m) is equal to 8500 Oe, and as can be seen at this magnetic field, both curves are saturated within a good accuracy, so the saturation magnetizations of the samples heated at 400 and 450°C are 3.4 and 2.4 emu/g, respectively.

In addition, it is clear from the inset of Figure 4 that when the applied magnetic field is zero, there are nonzero magnetizations, which are named residual ones. These remanent magnetizations are 0.34°emu/g and 0.15°emu/g for the samples heated at 400 and 450°C, respectively. Therefore, it is clear that like the saturation magnetization, the residual magnetization in the sample synthesized at 400°C is higher than that of the sample synthesized at 450°C. In order to

remove this residual magnetization from the samples, a specific magnetic field must be applied to the sample, which is called coercivity, and according to the inset of Figure 4, coercivities of these samples are 102.9 and 69.0 Oe, which again indicate that the amount of field required removing the remanent magnetization in the sample synthesized at 400°C is higher than that of the sample synthesized at 450°C.

3.2.1. BET Test. Based on the BET theory as well as the measured absorption and desorption values of the material, this system can calculate the specific surface area, diameter, volume, and size distribution of the pores of the material. The BET analysis works based on measuring the volume of nitrogen gas absorbed and desorbed by the material surface at a constant temperature of liquid nitrogen (77 K). In the BET test, after the cell containing the desired sample is placed in the liquid nitrogen tank, the amount of gas absorbed by the substance is calculated by gradually increasing the nitrogen gas pressure in each step. Then, by gradually reducing the gas pressure, the amount of desorption of the material is measured, and finally, the graph of the volume of nitrogen gas absorbed and desorbed by the material at a constant temperature is drawn [31]. According to equation (7), which is called the single-point method, V_m (the volume of nitrogen gas that is monomolecular adsorbed under standard surface conditions) can be obtained [32]:

$$v_m = v_a\left(1 - \frac{p}{p_0}\right). \tag{7}$$

In equation (7), V_a is the volume of absorbed gas in standard conditions, P_0 is the partial pressure of absorbed gas in the equilibrium state in Pascals, P is the partial pressure of absorbed gas in Pascals, and V_m (mL) is the volume of absorbed gas in standard conditions to produce a single layer on the surface of the sample. Therefore, the relation by plotting the changes of $P/(V\ (P_0–P))$ in terms of P/P_0, the slope obtained in the linear region will be proportional to V_m. With the value of V_m, the specific surface area of the substance (S_{BET}) can be obtained by the following equation:

$$S_{(BET)} = \frac{v_m N a}{m \times 22400}. \tag{8}$$

In equation (8), N is the Avogadro's number, m is the mass of the sample under test in grams, and a is the effective cross-sectional area of an adsorbed molecule in square millimeters (for nitrogen molecule equal to 0.162 nm^2). According to these equations, the value of the specific surface for the studied sample is equal to 25.2 $m^2.g^{-1}$

As seen in Figure 5, the size of the holes in this sample is mostly less than 10 nm, which proves that this material is microporous. Also, the volume of the holes obtained according to the BJH theory is equal to 14.4 $cm^3.g^{-1}$. In addition, the mean diameter of the holes for this sample is equal to 2.297 nm.

The Barrett–Joyner–Halenda (BJH) method was used to check the hole size distribution and the result is shown in Figure 4. As seen in Figure 5, the size of the holes in this

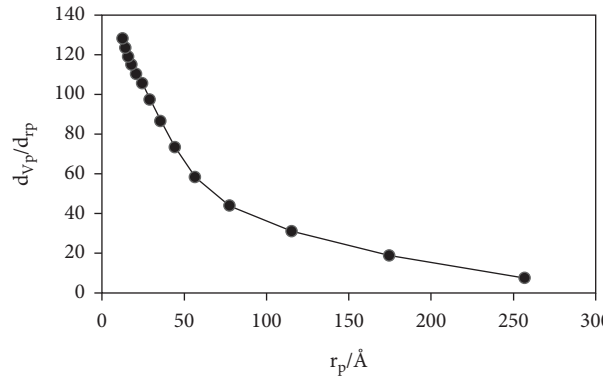

Figure 5: Size distribution of pores measured according to BJH theory for the TWMNPs.

sample is mostly less than 10 nm, which proves that this material is microporous. Also, the volume of the holes obtained according to the BJH theory is equal to 14.4 $cm^3.g^{-1}$. In addition, the mean diameter of the holes for this sample is equal to 2.297 nm.

In order to check the type and mechanism of absorption, the curve of nitrogen absorption/desorption changes in liquid nitrogen (temperature 77 K) is shown in Figure 6(a).

According to the result shown in Figure 6(a), the adsorption isotherm for the examined sample follows model III (according to IUPAC classification) [33, 34] (Figure 6(a)), and has a narrow hysteresis loop in the P/P_0 ratio of about 0.50 to 1. In this model, as it is clear in Figure 6(a), absorption is low at low pressures, but after a certain pressure, adsorption increases strongly. The Freundlich model is usually observed for nonporous adsorbents, whose adsorption is weak at first, and as mentioned, this weakness causes little adsorption at first, but when a certain number of adsorbed molecules are adsorbed by the adsorbent, the adsorption forces lead to the tendency of other molecules to be absorbed increases and the absorption increases exponentially after the formation of the first layer, so that as the pores are filled and the adsorbent is condensed on the surface, and the rate of absorption increases significantly [35, 36].

The existence of mesopores is in accordance with the BET classification. In addition, the BET analysis shows the specific surface area of the prepared magnetite nanoparticles 25.2 $m^2.g^{-1}$ of the adsorbent (Figure 6(b)). The results of the dBJH analysis showed that the pore volume (V_P) of TWMNPs was 0.13 cm^3g^{-1} of the adsorbent, and the maximum pore radius was 1.3 nm (Figure 7(a)). The calculation of adsorbent pore size distribution was determined using the BJH method. The BJH analysis of magnetite nanoparticles is shown in Figure 7(b). The M_P analysis showed that total volume of adsorbent pores is 0.3 $cm^3.g^{-1}$ of the adsorbent. Also, the mean pore diameter was 0.68 nm, Figure 7(c).

3.2.2. The Effect of Pb (II) Initial Concentration. The removal of Pb (II) on TWMNPs as a function of their concentrations was studied at a constant temperature (25 ± 0.1°C) by varying

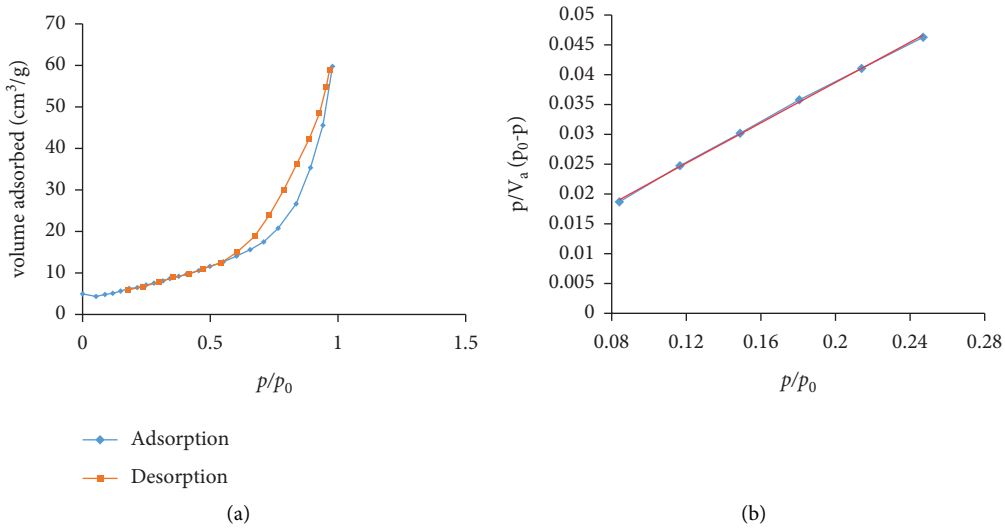

Figure 6: (a) N_2adsorption-desorption isotherms and (b) BET plot TWMNPs.

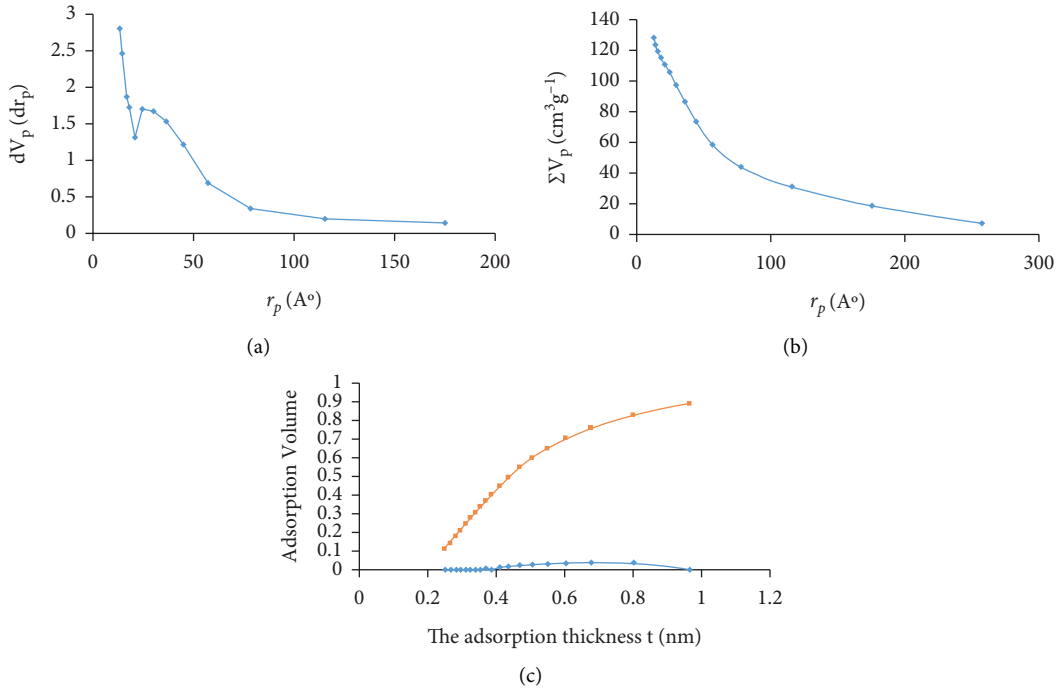

Figure 7: (a) dBJH plot, (b) BJH plot, and (c) MP plot TWMNPs.

the Pb (II) concentration from 100 to 200 mg L^{-1} while keeping all other parameters constant. The adsorption results of Pb (II) by tea wastes are shown in Figure 8(a).

According to Figure 8(a), with increasing the initial concentration of Pb (II) (Cp) from 0.1 to 2 g L^{-1}, the amount of Pb (II) removal and the response surface increased. One of the most important causes for the increase in Pb (II) adsorption is the increasing pressure gradient and driving force in mass transfer and as a result Pb (II) adsorption by magnetite nanoparticles increases [26]. In a research project by Zhang et al., the deletion of Pb (II) by SiO_2-Fe_3O_4 and AlOOH was examined, their results showed that lead removal increased with increasing initial Pb (II) concentration [37]. Similarly, Nassar et al. showed the amount of Pb (II) adsorption increased as the initial concentration of Pb (II) ions increased [38].

3.2.3. Effects of pH. Aqueous solution's pH is one of the important controlling parameters in the adsorption because it influences the degree of ionization of the adsorbate during the reaction, concentration of the counter ions on the functional groups of the adsorbent, and the solubility of the metal ions during the adsorption process [20, 39].

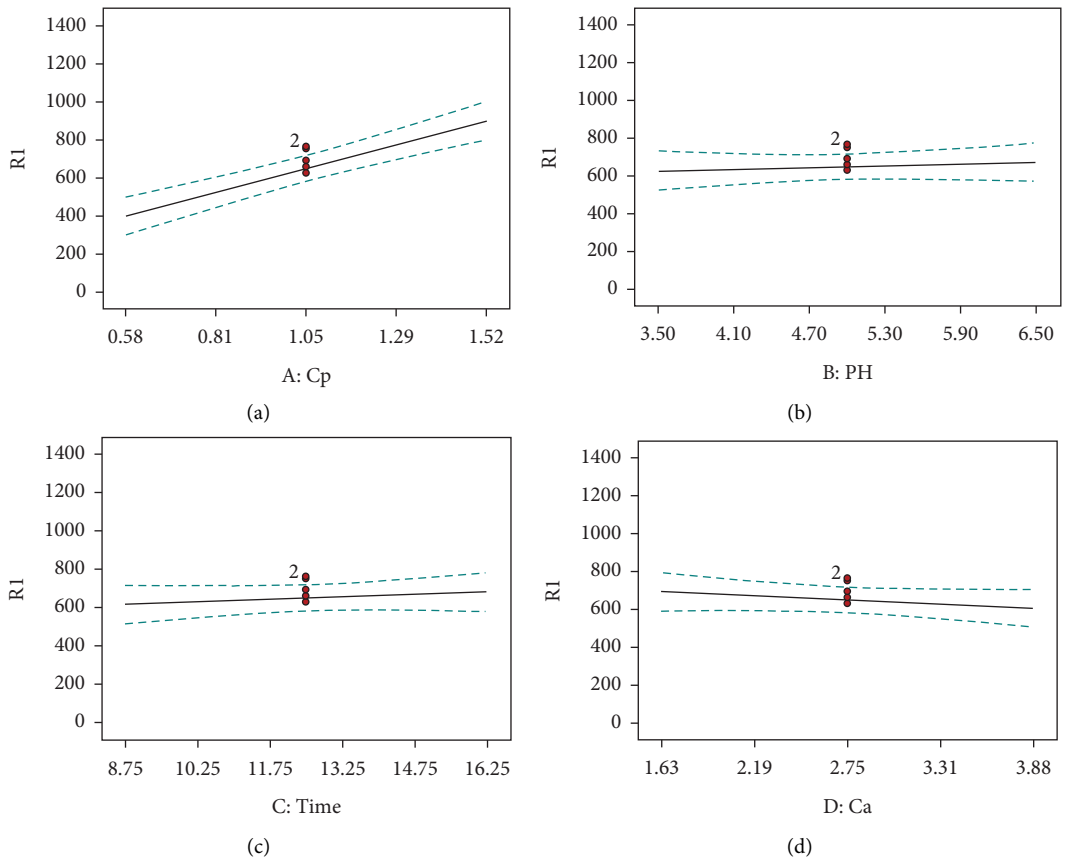

Figure 8: (a) Effects of initial concentration Pb (II), (b) pH, (c) nano adsorbent dosage, and (d) contact time on Pb (II) removal rate.

Therefore, the effect of pH on the adsorption of Pb (II) ions by TWMNPs adsorbent in the range of 3.5–6.5 was studied, the results are shown in Figure 8(b). All the variables, such as, adsorbent dosage, rpm, contact time, and temperature were kept constant, for the modification with magnetite nanoparticle with tea waste (Fe_3O_4–TW), the uptake efficiency gradually increases as the pH increases from 3.5 to 6.5. At lower pH, the concentration of H^+ ion is high, causing a competition for a vacant adsorbent site between the H^+ ion and Pb (II) cations. According to the obtained results as pH increases, the response surface and removal efficiency of Pb (II) increased. Because at high pH, the surface groups of hydroxyl have a negative charge and cause the absorption of cations [40]. Similar results were observed by Zhang et al., Katlego et al., and Wang et al., when they studied the removal of Pb (II) from an aqueous solution by fried egg jellyfish hydroxyapatite/magnetite composite adsorbent and activated carbon, respectively [37, 39, 41].

3.2.4. Effects of Contact Time. Results obtained in Figure 8(c) show that time is one of the important factors affecting the amount of the metal adsorbed by the nanoparticle. Obviously, these materials have very large surfaces compared to other absorbents. As a result, these can remove enormous amounts of water-soluble metals [4].

As can be observed in Figure 8(c) with increasing contact time, the removal efficiency of lead increased. At the beginning of the process, lead was quickly removed by the absorbent. Having a large number of free sites on the adsorbent surfaces at the beginning of the reactions was another reason for quick absorption. In other words, the less-saturating active sites on the absorbent lead to an increase in the speed of collision between metal ions and adsorption sites. Results of another study conducted by Dargahi et al., Gupta et al., and Atieh et al. on Pb and Cr removal from aqueous solution using the nanoparticles absorbent confirm our results [4, 42, 43].

3.2.5. The Effect of Nano Adsorbent Dosage. By increasing the amount of nanoadsorbent dosage (Ca) in the range of 0.5 to 4 g L^{-1}, the amount of Pb (II) removal and also the response surface (R_1) increased. As the adsorbent concentration increases, the number of particles around the Pb (II) ion increases too, and decreasing the amount of Pb (II) removal by increasing the adsorbent concentration is due to the gap in the concentration gradient between the solute concentration in the solution and the surface of the sorbent, Figure 8(d) [44]. In a study, Heather Shipley et al. investigated the efficiency of Pb (II) removal by hematite nanoparticles that obtained different results [45]. Rajput et al., in their study, examined the Pb (II) and Cr removal

from water by magnetite nanoparticles and showed different results from our results [46].

3.2.6. Simultaneous Effects of Variables on Lead Removal. The effects of initial Pb (II) concentration and initial pH on the Pb (II) removal rate are shown in Figure 9(a). The initial concentration of Pb (II) varied from 0.5 to 2 g L^{-1} and the initial pH varied from 3.5 to 6.5. The adsorbent concentration and contact time were considered constant at 2.75 g L^{-1} and 10 min, respectively. According to Figure 9(b), with increasing both the initial Pb (II) concentration and initial pH, the process efficiency increases. So that the response level of 400 in concentration (0.58 g L_{-1} Pb(II), pH = 3.5), increased to 900 at the concentration (1.52 g.L_{-1} Pb(II), pH = 6.5). The simultaneous effect of initial Pb (II) concentration and contact time on Pb (II) removal rate are shown in Figure 9(b).

The initial concentration of Pb (II) varied from 0.5 to 2 g L^{-1} and the contact time varied from 8.75 to 16.25. Also, the adsorbent concentration and Pb were considered constant at 2.75 g L^{-1} and 6, respectively According to the figure, with increasing the initial Pb (II) concentration and contact time, the response surface increases to 850 at a concentration of 1.52 g L^{-1} Pb (II) and contact time of 16.25 min.

The simultaneous effect of the initial concentration of Pb (II) and the adsorbent concentration in Figure 9(c) showed that at constant pH and contact time in 6 and 16 min, respectively. With increasing the concentration of Pb from 0.58 g L^{-1} to 1.52 g L^{-1} and increasing the adsorbent concentration from 1.63 g L^{-1} to 3.88 g L^{-1}, the response surface of Pb (II) increases to 900. According to the obtained results, high values of removal efficiency can be achieved in different conditions. Although with increasing the adsorbent dose, the removal efficiency of lead decreases, but with increasing the initial concentration of the contaminant, the removal efficiency can be increased. Also, increasing the contact time has a slight effect on the response surface, but with the simultaneous increase of the initial concentration of lead, the removal efficiency increases significantly.

3.2.7. Adsorption Isotherm. Adsorption isotherm is one of the important factors in designing the adsorption systems. In this research, two Langmuir and Freundlich adsorption isotherm models were investigated. The results of adsorption isotherms and parameters calculated from two models are shown in Table2 and Figure 10. In order to determine the absorption capacity of an adsorbent, this parameter is an important and effective factor. In order to determine the adsorption mechanism, Langmuir and Freundlich isotherms were used in this research [47, 48]. The linear equation of the Langmuir isotherm is given in equations (9) and (10).

$$\frac{C_e}{q_e} + \frac{1}{q_m \times b} + \frac{C_e}{q_m}, \tag{9}$$

where q_e (mg.g^{-1}) is the equilibrium adsorption capacity of TWMNPs, C_e (mg.L^{-1}) is the equilibrium concentration of Pb (II) ion in the solution, q_m (mg.g^{-1}) is the maximum adsorption capacity, and b is the Langmuir constant that is obtained in the curve (C_e/q_e) *vs.* C_e. The linear equation of the Freundlich isotherm is given in the following (Equation (10)).

$$\log q_e - \log K = \frac{1}{n}\log C_e, \tag{10}$$

where q_e is the equilibrium adsorption capacity in mg.g^{-1}. The equilibrium concentration of the adsorbent is expressed as, C_e, in mg.L^{-1} and K and n are the Freundlich constants obtained in the curve.

Here, q_e(mg.g^{-1}) is the equilibrium adsorption capacity. C_e(mg.L^{-1}) is the equilibrium concentration of the adsorbent, and K and n are the Freundlich constants obtained in the curve logqe vs. logCe [47, 48]. The results showed that the adsorption in TWMNPs follows the Langmuir model ($R^2 = 0.963$), and the maximum adsorption capacity of Pb (II) on to the TWMNPs at 10.67 mg.g^{-1} indicated the ability of the TWMNPs for adsorption of Pb (II).

Compared to the uptake by the adsorbate employed in previous studies indicated the ability of the TWMNPs for adsorption of Pb (II), and the TWMNPs adsorbent utilized in this investigation exhibited good dish Pb (II) removal capabilities (see Table 3).

3.2.8. Adsorption Kinetics. Reaction kinetics provide a measurement of reaction rates, factors that affect the rate of a chemical reaction and insight into reaction mechanisms. The rate equations actually show the relationship between concentration and time. The rate of production of products in a zero-order reaction is independent of the amount of reactants. In first-order reactions, the removal rate depends on the initial concentration of the reactant, and the reaction rate is proportional to the initial concentration of the reactant. However, the second order reactions can be defined as chemical reactions in which the sum of powers in the corresponding rate law of the chemical reaction is equal to [47]. The kinetic equations are shown in Table 4.

Reactant concentration at time C_0 (mg.L^{-1}) (primary reactant concentration), C_t (mg.L^{-1}), reactant concentration at time t, and reaction rate constant k. In zero, first-, and second-order equations, [C_t], (Ln[C_t]/[C_0]), and (1/[C_t]), respectively, are plotted against time to determine the rate constant (Table 5).

The correlation coefficients are provided in Table 4. Based on the results, the process kinetics of TWMNPs were of the first-order type.

Table 6 shows the comparison of this method with other methods in removing lead metal.

3.2.9. Pareto Chart. A Pareto chart is a graph that indicates the frequency of defects, as well as their cumulative impact. Pareto charts are useful to find the defects to prioritize in order to observe the greatest overall improvement. Figure 11 shows the Pareto diagram for different parameters. Based on the observed results, in this study, the first important variable is the concentration of pollutants, Table 6.

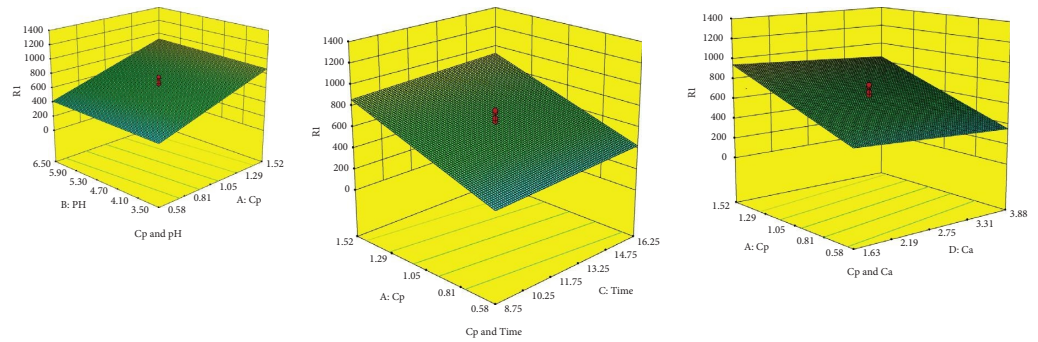

(a) (b) (c)

Figure 9: Simultaneous effects of initial concentration of Pb (II) and pH (a), initial concentration of Pb (II) and adsorbent concentration on Pb (II) removal rate (b) and, initial concentration of Pb (II) and contact time (c).

Table 2: Parameter isotherms of adsorption for the Langmuir and Freundlich-TWMNPs.

Isotherms	Isotherm equations	Fixed coefficients and correlation coefficients of isotherms		
Langmuir	$(1/q_e) = (1/q_m k_L C_e) + (1/q_m)$	q_m (mg.g^{-1})	R^2	K_L
		10.67	0.963	1.125
Freundlich	$\text{Log}q_m = \text{Log}K + (1/n)\text{Log}C_e$	K	$(1/n)$	R^2
		0.619	2.180	0.772

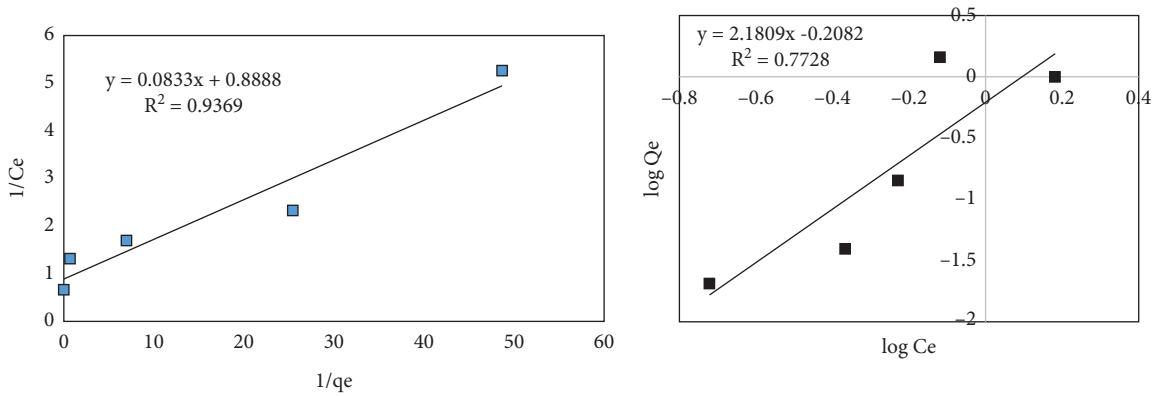

(a) (b)

Figure 10: Pb (II) adsorption isothermal models by TWMNPs: (a) Langmuir and (b) Freundlich.

Table 3: Adsorption capacities q_{max} (mg/g) for Pb (II) of various adsorbents.

Adsorbents	Adsorbate	q_{max} (mg/g)	Removal efficiency (%)	References
Nano maghemite	Pb (II)	61	63	[49]
Magnetite iron nanoparticles	Pb (II)	1.319×10^{-3}	70	[50]
Fe_3O_4-tea waste	Ni (II)	38	87–99	[20]
Rice straw	Pb (II)	23.3	97	[51]
Tea pulp modified with magnetite nanoparticles (TWMNPs)	Pb (II)	10.67	90	Current study

Table 4: Correlation coefficient values of adsorption rate equations for TWMNPs.

Order	Correlation coefficient	Speed constant (1 min^{-1})
Zero	0.898	0.0851
First	0.914	0.1404
Second	0.764	0.3185

Table 5: Kinetics equations.

Order	Equation	Linear model
Zero	$[C_t - C_0] = -kt$	$[C_t]$
First	$\text{Ln}([C_t]/[C_0]) = kt$	$\text{Ln}([C_t]/[C_0])$
Second	$\text{Ln}([1/C_t] - [1/C_0]) = kt$	$([1/C_t])$

Table 6: Comparing the use of magnetic iron nanoparticles with other methods in removing Pb (II) from wastewater.

Parameters	Magnetic iron nanoparticles [52–54]	Chemical and physical [55, 56]	Biologically [57–59]
Temperature	Environment temperature (25 C)	Environment temperature (25 C)	15–22 (C)
Lead recycling	Recyclable	Nonrecyclable	Nonrecyclable
Sludge control	No sludge production	Production of high volumes of sludge	Production of high volumes of sludge
Pollution load	Ability to treatment wastewater with high pollution load	Ability to treatment wastewater with high pollution load	Ability to treatment wastewater with low pollution load
Energy consumption	Low	High	High
The cost of treatment	Low	High (cost of chemicals)	High
Reusability	Excellent	No	No

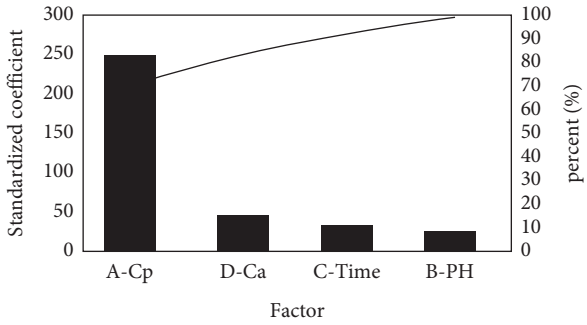

Figure 11: Pareto chart to determine the effect of factors.

4. Conclusions

This study showed that tea-treated magnetite nanosorbents can be used as an effective adsorbent for adsorption of Pb (II) from the industrial wastewater. The results showed that with increasing the pH from 3.5 to 6.5, a slight increase in the response surface was observed. With increasing the initial concentration of Pb (II) from 0.1 to 2 g L^{-1}, the amount of Pb (II) removal and response surface increased and maximum removal was obtained at a concentration of 1.52 g L^{-1}. Adsorption was highly dependent on the initial concentration of Pb (II). Optimum nanosorbents to achieve the desired Pb (II) removal was 1.63 g L^{-1}, with increasing contact time from 5 to 16 min, the response surface increased slightly. The optimal contact time for Pb (II) removal was 8.75 min. The specific surface area of the prepared nanoparticles was 25.2 $m^2.g^{-1}$ of adsorbent. Because magnetite nanoparticles can be separated from an aqueous solution by a permanent magnet easily, it is environmentally suitable as an alternative method for effective removal of lead from wastewater than other expensive methods. The adsorption data were well fitted by the Langmuir isotherm. The adsorption capacity was found to be 10.67 $mg.g^{-1}$. The kinetics of adsorption followed first-order kinetics.

In conclusion, we presented a simple and cost-effective method for obtaining magnetic Fe_3O_4 nanoparticles from tea waste modified with magnetic nanoparticles (TWMNPs) and using them to remove Pb from wastewater. The crystalline nature of Fe_3O_4 nanoparticles is improved by tea waste. TWMNPs demonstrated an excellent ability to remove Pb from wastewater.

Abbreviation

TWMNPs: Tea waste modified with magnetite nanoparticles
DDW: Double distilled water
XRD: X-ray diffraction (XRD)
VSM: Vibrating-sample magnetometer
RSM: Response surface methodology
CCD: Central composite design
BET: Brunauer–Emmett–Teller
BJH: Barrett–Joyner–Halenda
MP: Micropore
V_m: Volume of absorbed gas
N: Avogadro's number
IUPAC: International Union of Pure and Applied Chemistry
a: The effective cross-sectional area of an adsorbed molecule atomic absorption spectrophotometer limit of detection
AAS: Atomic absorption spectrophotometer
LoD: Limit of detection
FESEM: Field emission scanning electron microscopy
K: Shape factor
λ: Wavelength of X-ray
FWHM: Full width at half maximum
JCPDS: Joint Committee on Powder Diffraction Standards
Hm: Maximum applied field
Mr/Ms: Squareness ratio, remanent magnetization (remanence)/saturation magnetization
V_p: Pore volume
Va: Volume of absorbed gas in standard conditions
P_0: The partial pressure of absorbed gas in the equilibrium state
R_1: Response surface
WHO: World Health Organization
EPA: Environmental Protection Agency
Å: Angstrom
LoQ: Limit of quantitation.

Data Availability

The data used to support the findings of this study are included within the article.

Conflicts of Interest

The authors declare that they have no conflicts of interest.

Acknowledgments

The authors would like to acknowledge the support provided by the Department of Materials Engineering, Naqsh Jahan Institute of Higher Education, Isfahan, Iran.

Supplementary Materials

The graphical abstract of the article has been included in the supplementary materials. (*Supplementary Materials*)

References

[1] S. Gunatilake, "Methods of removing heavy metals from industrial wastewater," *Methods*, vol. 1, no. 1, p. 14, 2015.
[2] N. M. Mubarak, J. N. Sahu, E. C. Abdullah, and N. S. Jayakumar, "Removal of heavy metals from wastewater using carbon nanotubes," *Separation and Purification Reviews*, vol. 43, no. 4, pp. 311–338, 2014.
[3] A. Azimi, A. Azari, M. Rezakazemi, and M. Ansarpour, "Removal of heavy metals from industrial wastewaters: a review," *ChemBioEng Reviews*, vol. 4, no. 1, pp. 37–59, 2017.
[4] A. Dargahi, H. Gholestanifar, P. Darvishi et al., "An investigation and comparison of removing heavy metals (lead

and chromium) from aqueous solutions using magnesium oxide nanoparticles," *Polish Journal of Environmental Studies*, vol. 25, no. 2, pp. 557–562, 2016.

[5] M. Arbabi, S. Hemati, and M. Amiri, "Removal of lead ions from industrial wastewater: a review of Removal methods," *International Journal of Epidemiologic Research*, vol. 2, no. 2, pp. 105–109, 2015.

[6] J. Acharya, U. Kumar, and B. Meikap, "Thermodynamic characterization of adsorption of lead (II) ions on activated carbon developed from tamarind wood from aqueous solution," *South African Journal of Chemical Engineering*, vol. 18, no. 1, pp. 70–76, 2013.

[7] S. Abdel-Halim, A. Shehata, and M. El-Shahat, "Removal of lead ions from industrial waste water by different types of natural materials," *Water Research*, vol. 37, no. 7, pp. 1678–1683, 2003.

[8] M. Mondal, "Removal of Pb (II) ions from aqueous solution using activated tea waste: adsorption on a fixed-bed column," *Journal of Environmental Management*, vol. 90, no. 11, pp. 3266–3271, 2009.

[9] H. Taghipour and M. Mosaferi, "Heavy metals in the vegetables collected from production sites," *Health Promotion Perspectives*, vol. 3, no. 2, pp. 185–193, 2013.

[10] F. M. Alzahrani, N. S. Alsaiari, K. M. Katubi et al., "Magnetic nitrogen-doped porous carbon nanocomposite for Pb (II) adsorption from aqueous solution," *Molecules*, vol. 26, no. 16, p. 4809, 2021.

[11] S. Moradinasab and M. Behzad, "Removal of heavy metals from aqueous solution using Fe3O4 nanoparticles coated with Schiff base ligand," *Desalination and Water Treatment*, vol. 57, no. 9, pp. 4028–4036, 2016.

[12] M. A. A. Wijayawardena, M. Megharaj, and R. Naidu, "Bioaccumulation and toxicity of lead, influenced by edaphic factors: using earthworms to study the effect of Pb on ecological health," *Journal of Soils and Sediments*, vol. 17, no. 4, pp. 1064–1072, 2017.

[13] H. Hashemi, A. Khodabakhshi, B. Alinia, and F. Abbasi, "Bioremediation of lead and zinc contaminated soils by compost worm," *Journal of Health Sciences and Surveillance System*, vol. 6, no. 2, pp. 58–63, 2018.

[14] A. Ramezanpoor, A. Farrokhian Firouzi, G. Sayyad, and A. Kiyasat, "Investigation of Pb (II) removal from aqueous solutions using modified nano zero-valent iron particles," *Journal of Water and Wastewater; Ab va Fazilab (in persian)*, vol. 25, no. 2, pp. 68–76, 2014.

[15] L. Dong, Z. Zhu, Y. Qiu, and J. Zhao, "Removal of lead from aqueous solution by hydroxyapatite/magnetite composite adsorbent," *Chemical Engineering Journal*, vol. 165, no. 3, pp. 827–834, 2010.

[16] S. R. Kanel and H. Choi, "Removal of arsenic from groundwater by industrial byproducts and its comparison with zero-valent iron," *Journal of Hazardous, Toxic, and Radioactive Waste*, vol. 21, no. 3, Article ID 04016028, 2017.

[17] S. Li, W. Wang, F. Liang, and W.-x. Zhang, "Heavy metal removal using nanoscale zero-valent iron (nZVI): theory and application," *Journal of Hazardous Materials*, vol. 322, pp. 163–171, 2017.

[18] A. H. Lu, E. L. Salabas, and F. Schüth, "Magnetic nanoparticles: synthesis, protection, functionalization, and application," *Angewandte Chemie International Edition*, vol. 46, no. 8, pp. 1222–1244, 2007.

[19] R. Kodama, "Magnetic nanoparticles," *Journal of Magnetism and Magnetic Materials*, vol. 200, no. 1-3, pp. 359–372, 1999.

[20] P. Panneerselvam, N. Morad, and K. A. Tan, "Magnetic nanoparticle (Fe3O4) impregnated onto tea waste for the removal of nickel (II) from aqueous solution," *Journal of Hazardous Materials*, vol. 186, no. 1, pp. 160–168, 2011.

[21] U. Schwertmann and R. M. Cornell, *Iron Oxides in the Laboratory: Preparation and Characterization*, John Wiley and Sons, Hoboken, NJ, USA, 2008.

[22] M. M. Rahman, S. B. Khan, A. Jamal, M. Faisal, and A. M. Aisiri, "Iron oxide nanoparticles," *Nanomaterials*, vol. 3, pp. 43–67, 2011.

[23] O. Akhavan, M. Kalaee, Z. Alavi, S. Ghiasi, and A. Esfandiar, "Increasing the antioxidant activity of green tea polyphenols in the presence of iron for the reduction of graphene oxide," *Carbon*, vol. 50, no. 8, pp. 3015–3025, 2012.

[24] W. H. Organization, *Lead in Drinking-Water: Background Document for Development of WHO Guidelines for Drinking-Water Quality*, World Health Organization, Geneva, Switzerland, 2003.

[25] S. Lunge, S. Singh, and A. Sinha, "Magnetic iron oxide (Fe3O4) nanoparticles from tea waste for arsenic removal," *Journal of Magnetism and Magnetic Materials*, vol. 356, pp. 21–31, 2014.

[26] A. Khodabakhshi and H. Asgarian, "Removal of mercury (II) from aqueous solutions by multiwalled carbon nanotubes coated with manganese oxide," *Journal of Shahrekord University of Medical Sciences*, vol. 21, no. 6, pp. 258–264, 2019.

[27] A. Dargahi, M. Vosoughi, S. Ahmad Mokhtari, Y. Vaziri, and M. Alighadri, "Electrochemical degradation of 2, 4-Dinitrotoluene (DNT) from aqueous solutions using three-dimensional electrocatalytic reactor (3DER): degradation pathway, evaluation of toxicity and optimization using RSM-CCD," *Arabian Journal of Chemistry*, vol. 15, no. 3, Article ID 103648, 2022.

[28] M. M. Amin, A. Khodabakhshi, M. Mozafari, B. Bina, and S. Kheiri, "Removal of Cr (VI) from simulated electroplating wastewater by magnetite nanoparticles," *Environmental Engineering and Management Journal*, vol. 9, no. 7, pp. 921–927, 2010.

[29] A. M. Atta, H. A. Al-Lohedan, and S. A. Al-Hussain, "Synthesis of stabilized myrrh-capped hydrocolloidal magnetite nanoparticles," *Molecules*, vol. 19, no. 8, pp. 11263–11278, 2014.

[30] F. Hajipour, S. Asad, M. A. Amoozegar et al., "Developing a fluorescent hybrid nanobiosensor based on quantum dots and azoreductase enzyme for methyl red monitoring," *Iranian Biomedical Journal*, vol. 25, no. 1, pp. 8–20, 2021.

[31] F. Ambroz, T. J. Macdonald, V. Martis, and I. P. Parkin, "Evaluation of the BET theory for the characterization of meso and microporous MOFs," *Small Methods*, vol. 2, no. 11, Article ID 1800173, 2018.

[32] B. Coasne, K. E. Gubbins, and R. M. Pellenq, "A grand canonical Monte Carlo study of adsorption and capillary phenomena in nanopores of various morphologies and topologies: testing the BET and BJH characterization methods," *Particle and Particle Systems Characterization*, vol. 21, no. 2, pp. 149–160, 2004.

[33] C. Buttersack, "Modeling of type IV and V sigmoidal adsorption isotherms," *Physical Chemistry Chemical Physics*, vol. 21, no. 10, pp. 5614–5626, 2019.

[34] M. M. Rahman, M. Muttakin, A. Pal, A. Z. Shafiullah, and B. B. Saha, "A statistical approach to determine optimal models for IUPAC-classified adsorption isotherms," *Energies*, vol. 12, no. 23, p. 4565, 2019.

[35] C. De Smedt, F. Ferrer, K. Leus, and P. Spanoghe, "Removal of pesticides from aqueous solutions by adsorption on zeolites as solid adsorbents," *Adsorption Science and Technology*, vol. 33, no. 5, pp. 457–485, 2015.

[36] F. J. Sotomayor, K. A. Cychosz, and M. Thommes, "Characterization of micro/mesoporous materials by physisorption: concepts and case studies," *Accounts of Material Surface Research*, vol. 3, no. 2, pp. 34–50, 2018.

[37] Y.-X. Zhang, X.-Y. Yu, Z. Jin et al., "Ultra high adsorption capacity of fried egg jellyfish-likeγ-AlOOH (Boehmite)@ SiO2/Fe3O4 porous magnetic microspheres for aqueous Pb (II) removal," *Journal of Materials Chemistry*, vol. 21, no. 41, pp. 16550–16557, 2011.

[38] N. N. Nassar, "Rapid removal and recovery of Pb (II) from wastewater by magnetic nanoadsorbents," *Journal of Hazardous Materials*, vol. 184, no. 1-3, pp. 538–546, 2010.

[39] S. Katlego, R. Jianwei, A. Ochieng, and S. O. Maurice, "Removal of Pb (II) from aqueous solution using hydrotalcite-like nanostructured material," *International Journal of the Physical Sciences*, vol. 7, no. 1, pp. 63–72, 2012.

[40] A. Pranudta, N. Chanthapon, P. Kidkhunthod, M. M. El-Moselhy, T. T. Nguyen, and S. Padungthon, "Selective removal of Pb from lead-acid battery wastewater using hybrid gel cation exchanger loaded with hydrated iron oxide nanoparticles: fabrication, characterization, and pilot-scale validation," *Journal of Environmental Chemical Engineering*, vol. 9, no. 5, Article ID 106282, 2021.

[41] L. Wang, J. Zhang, R. Zhao, Y. Li, C. Li, and C. Zhang, "Adsorption of Pb (II) on activated carbon prepared from Polygonum orientale Linn.: kinetics, isotherms, pH, and ionic strength studies," *Bioresource Technology*, vol. 101, no. 15, pp. 5808–5814, 2010.

[42] V. Gupta, S. Agarwal, and T. A. Saleh, "Chromium removal by combining the magnetic properties of iron oxide with adsorption properties of carbon nanotubes," *Water Research*, vol. 45, no. 6, pp. 2207–2212, 2011.

[43] M. A. Atieh, "Effect of functionalized carbon nanofibers with carboxylic function group on the removal of zinc from water," *International Journal of Environment and Sustainable Development*, vol. 2, no. 2, pp. 142–145, 2011.

[44] V. Vadivelan and K. V. Kumar, "Equilibrium, kinetics, mechanism, and process design for the sorption of methylene blue onto rice husk," *Journal of Colloid and Interface Science*, vol. 286, no. 1, pp. 90–100, 2005.

[45] H. J. Shipley, K. E. Engates, and V. A. Grover, "Removal of Pb (II), Cd (II), Cu (II), and Zn (II) by hematite nanoparticles: effect of sorbent concentration, pH, temperature, and exhaustion," *Environmental Science and Pollution Research*, vol. 20, no. 3, pp. 1727–1736, 2013.

[46] S. Rajput, C. U. Pittman, and D. Mohan, "Magnetic magnetite (Fe3O4) nanoparticle synthesis and applications for lead (Pb2+) and chromium (Cr6+) removal from water," *Journal of Colloid and Interface Science*, vol. 468, pp. 334–346, 2016.

[47] A. Khodabakhshi, F. Mohammadi-Moghadam, K. Shakeri, and S. Hemati, "Equilibrium and thermodynamic studies on the biosorption of lead (II) by living and nonliving biomass of penicillium notatum," *Journal of Chemistry*, vol. 2022, Article ID 3109212, 9 pages, 2022.

[48] A. Khodabakhshi, F. Mohammadi-Moghadam, M. M. Amin, S. Hamati, and S. Hayarian, "Comparison of paraquat herbicide removal from aqueous solutions using nanoscale zero-valent iron-pumice/diatomite composites," *International Journal of Chemical Engineering*, vol. 2021, Article ID 4319660, 12 pages, 2021.

[49] A. Khodabakhshi, M. kamali, M. Amin, M. Sedehi, M. Hadialijanvand, and M. Vahid Dastjerdi, "Lead removal from battery industry synthetic wastewater by nano maghemite," *Journal of Health System Research*, vol. 11, no. 1, pp. 132–142, 2015.

[50] R. Alizadeh, S. Abedini, N. Bidhendi, and G. Amoabediny, "Removal of lead from battery manufacture industry wastewater by magnetite iron nano particles," *Nashrieh Shimi va Mohandesi Shimi Iran*, vol. 30, no. 1, pp. 71–77, 2011.

[51] S. Sepehri, E. Kanani, S. Abdoli, V. D. Rajput, T. Minkina, and B. Asgari Lajayer, "Pb (II) removal from aqueous solutions by adsorption on stabilized zero-valent iron nanoparticles—a green approach," *Water*, vol. 15, no. 2, p. 222, 2023.

[52] T. Luo, C. Yang, X. Tian, W. Luo, Y. Nie, and Y. Wang, "Application of iron oxide nanomaterials for the removal of heavy metals," *Handbook of Nanomaterials and Nanocomposites for Energy and Environmental Applications*, Springer, Berlin, Germany, 2020.

[53] S. Rahmani, B. Beheshti, and M. R. Doosti, "Removal of cobalt from contaminated water using magnetic iron oxide nanoparticles," *Amirkabir Journal of Civil Engineering*, vol. 53, no. 1, pp. 213–228, 2021.

[54] A. Moezzi, S. Soltanali, A. Torabian, and A. Hassani, "Removal of lead from aquatic solution using synthesized iron nanoparticles," *International Journal of NanoScience and Nanotechnology*, vol. 13, no. 1, pp. 83–90, 2017.

[55] O. M. Themba, M.-M. Lizzy, N. M. Maggie, and B. M. Bhekie, "A simplified cost-effective biosand filter (BSFZ) for removal of chemical contaminants from water," *Journal of Chemical Engineering and Materials Science*, vol. 2, no. 10, pp. 156–167, 2011.

[56] H. Peng and J. Guo, "Removal of chromium from wastewater by membrane filtration, chemical precipitation, ion exchange, adsorption electrocoagulation, electrochemical reduction, electrodialysis, electrodeionization, photocatalysis and nanotechnology: a review," *Environmental Chemistry Letters*, vol. 18, no. 6, pp. 2055–2068, 2020.

[57] N. T. Abdel-Ghani, M. Hefny, and G. A. F. El-Chaghaby, "Removal of lead from aqueous solution using low cost abundantly available adsorbents," *International journal of Environmental Science and Technology*, vol. 4, no. 1, pp. 67–73, 2007.

[58] D. Bulgariu, G. Nacu, T. Măluan, and L. Bulgariu, "Kinetic study of lead (II) removal from aqueous solution onto lignin-based materials," *Cellulose Chemistry and Technology*, vol. 50, pp. 339–347, 2016.

[59] S. A. Razzak, M. O. Faruque, Z. Alsheikh et al., "A comprehensive review on conventional and biological-driven heavy metals removal from industrial wastewater," *Environmental Advances*, vol. 7, Article ID 100168, 2022.